Available online at www.sciencedirect.com
SCIENCE DIRECT
Polymer 46 (2005) 2646–2662
polymer
www.elsevier.com/locate/polymer

Nanocomposites from poly(ethylene-*co*-methacrylic acid) ionomers: effect of surfactant structure on morphology and properties

Rhutesh K. Shah[a,*], D.L. Hunter[b], D.R. Paul[a,*]

[a]*Department of Chemical Engineering and Texas Materials Institute, The University of Texas at Austin, Austin TX 78712, USA*
[b]*Southern Clay Products, 1212 Church St, Gonzales, TX 78629, USA*

Received 2 November 2004; received in revised form 26 January 2005; accepted 29 January 2005

Abstract

A detailed study of the structure–property relationships for nanocomposites prepared using melt processing techniques from a sodium ionomer of poly(ethylene-*co*-methacrylic acid) and a series of organoclays is reported. Transmission electron microscopy, X-ray scattering, stress-strain behavior, and Izod impact analysis were used to evaluate the nanocomposite morphology and physical properties. Four distinct surfactant structural effects lead to improved levels of exfoliation and higher stiffness for these nanocomposites: higher number of alkyl tails on the amine rather than one, longer alkyl tails instead of shorter ones, use of 2-hydroxy-ethyl groups as opposed to methyl groups on the ammonium ion, and an excess amount of the amine surfactant on the clay instead of an equivalent amount. These trends are opposite of what has been seen in nylon 6 based nanocomposites but are similar to those observed in nanocomposites formed from LDPE and LLDPE. Although some organoclays were exfoliated better than others, none of the ionomer-based nanocomposites exhibited exfoliation levels as great as those seen in nylon 6 nanocomposites; nevertheless, these nanocomposites offer promising improvements in performance and may be particularly interesting for barrier applications.

Keywords: Surlyn®; Ionomer; Nanocomposites

1. Introduction

The recent interest in polymer–organoclay nanocomposites stems from remarkable improvements in mechanical, thermal and barrier properties that have been demonstrated at low filler levels. The central scientific issue is how to achieve high levels of exfoliation of the nanometer thick clay platelets within the polymer matrix since this is necessary to realize the large filler aspect ratios that lead to the aforementioned improvements. The experimental approaches for improving clay exfoliation include optimization of processing conditions, selection of appropriate organoclays (surfactant treatment), and chemical modification of the polymer matrix to improve matrix-organoclay compatibility.

Polyamides seem to be one of the few polymer types which readily form well-exfoliated nanocomposites [1–5]. On the other hand, non-polar polymers like polyolefins seem incapable of exfoliating the organoclays by themselves, and addition of an appropriate compatibilizer or chemical modification of the polymer matrix is required. The grafting of maleic anhydride to the polyolefin backbone for use as the matrix polymer or as a compatibilizer significantly increases the polarity and, thus, improves exfoliation in polypropylene [6] and polyethylene [7–9]. Another approach is to copolymerize the olefin monomer with polar monomers like methacrylic acid [10] or acrylic acid. Ionomers, where some of the acid groups of such acid copolymers are neutralized to form sodium, zinc or magnesium salts offer an extension of this option. Besides improving the toughness and clarity of the polymer, the ionic groups also offer the possibility of favorable interactions with the organoclay. In the late nineties, Kobayashi et al. [11] and Hasegawa et al [12] were the first to report nanocomposites prepared from such ionomers.

* Corresponding authors. Tel.: +1 512 471 5392; fax: +1 512 471 0542.
E-mail addresses: rhutesh@che.utexas.edu (R.K. Shah), drp@che.utexas.edu (D.R. Paul).

0032-3861/$ - see front matter © 2005 Published by Elsevier Ltd.
doi:10.1016/j.polymer.2005.01.062

Table 1
Ionomers used in this study

Ionomer grade	MI (dg/min)	Methacrylic acid content (mol%)	Neutralization (%)	Sodium content (wt%)
Surlyn® 8920	0.9	5.53	44.1	1.78
Surlyn® 8940	2.8	5.81	27.0	1.14
Surlyn® 8945	4.0	5.59	39.0	1.58

Subsequently, ionomers of PP [13], PET [14,15], PBT [15,16], and a variety of thermoplastics [17–19] were used as matrices or compatibilizers to prepare nanocomposites.

The selection of a suitable organoclay is equally critical for producing nanocomposites with excellent exfoliation. Structural aspects of the surfactant like the number and length of alkyl tails, degree of saturation, etc. along with the amount of surfactant loading on the clay may significantly affect the degree of clay exfoliation [20–22]. Prior work [20,23] has shown that organic modifiers with one long alkyl tail lead to higher levels of organoclay exfoliation in nylon 6 than those having two alkyl tails. This is believed to be the result of the higher affinity that nylon 6 has for the pristine surface of the organoclay than for the largely aliphatic organic modifier. Similar trends were seen in SAN based nanocomposites [22]. On the other hand, nanocomposites made from a non-polar polymer like LLDPE showed completely opposite trends [7], i.e. the two-tailed organoclay formed nanocomposites with better exfoliation and mechanical properties than a one-tailed organoclay.

The objective of this study is to examine the effect of the number of alkyl tails and other aspects of the surfactant structure on the morphology and properties of nanocomposites made from poly(ethylene-*co*-methacrylic acid) ionomers. Specific comparisons among organic amine surfactants that are commercially available are made by addressing structural variations one issue at a time. Transmission electron microscopy (TEM), wide angle X-ray scattering (WAXS), stress–strain analysis and Izod impact measurements are used to evaluate nanocomposite morphology and physical properties.

2. Experimental

2.1. Materials

Three commercial grades of Surlyn® ionomer resins, Surlyn® 8920, 8940, and 8945 were purchased from du Pont. These are copolymers of ethylene and methacrylic acid where some of the acid groups are neutralized to form the sodium salt. The acid and sodium contents of these

Table 2
Organoclays used in this study

Organoclay	SCP designation	Chemical structure	Organic loading[a] (MER)	Organic content[b] (wt%)	d_{001} spacing[c] (Å)
$M_3(HT)_1$	Experimental	Trimethyl hydrogenated-tallow ammonium montmorillonite	95	29.6	18.0
$M_3(C_{18})_1$	Experimental	Octadecyl trimethyl ammonium montmorillonite	95	29.8	18.1
$M_3(C_{16})_1$	Experimental	Hexadecyl trimethyl ammonium montmorillonite	100	27.5	17.9
$M_2(HT)_2$-95	Cloisite® 20A[d]	Dimethyl bis(hydrogenated-tallow) ammonium montmorillonite	95	39.6	25.5
$M_2(HT)_2$-140	Cloisite® 6A[d]	Dimethyl bis(hydrogenated-tallow) ammonium montmorillonite	140	48.0	35.1
$M_1(C_{16})_3$	Experimental	Methyl trihexadecyl ammonium montmorillonite	100	43.4	29.3
$(HE)_2M_1C_1^*$	Experimental	bis(2-hydroxy-ethyl)methyl coco ammonium montmorillonite	95	26.4	14.4
$(HE)_2M_1T_1$	Cloisite® 30B[d]	bis(2-hydroxy-ethyl)methyl tallow ammonium montmorillonite	90	31.5	17.7
M_3T_1	Experimental	Trimethyl tallow quaternary ammonium montmorillonite	95	29.1	17.5
$M_1H_1(HT)_2$	Experimental	Methyl bis(hydrogenated-tallow) ammonium montmorillonite	95	38.4	24.3

[a] The organic loading describes the number of milliequivalents of amine salt used per 100 g of clay (MER) during the cation exchange reaction with sodium montmorillonite.
[b] The wt% of organic component on the final organoclay was determined by high temperature residual ash measurements.
[c] The basal spacing corresponds to the characteristic Bragg reflection peak (d_{001}) obtained from a powder WAXS scan of the organoclay.
[d] Cloisite® is a registered trademark of Southern Clay Products, Inc.

polymers were determined from oxygen and sodium elemental analyses with the results listed in Table 1.

Organoclays used in this study were prepared by an ion exchange reaction between sodium montmorillonite (Na-MMT) and amine surfactants and were supplied by Southern Clay Products, Inc. The organoclays selected for this study are listed in Table 2 along with their *d*-spacings (determined by X-ray analysis) and the cation exchange amount expressed as the milliequivalent ratio (MER). The amine surfactants are derived from natural products like coconut and tallow oils. Details of the chemical composition of these natural products are available in the literature [24]. A nomenclature system, similar to that used in prior papers [20,21], has been adopted to describe the amine structure in a concise manner, i.e., M for methyl, H for hydrogen, (HE) for 2-hydroxy-ethyl, C* for coconut oil (predominantly C_{12} chains), T for tallow oil (predominantly C_{18} chains), and HT for hydrogenated tallow oil (saturated). Procedural details of the cation exchange reaction between the onium ions and Na-MMT are provided by Fornes et al. [20].

The organoclays were carefully chosen to explore the effect of the chemical structure of the surfactant on the extent of organoclay exfoliation observed in the corresponding Surlyn® based nanocomposites made using them. This series compares one at a time the effects of the number of alkyl tails, length of alkyl tails, hydroxy-ethyl versus methyl substituents, quaternary versus tertiary ammoniums, degree of saturation and level of organic loading.

2.2. Melt processing

Melt compounded composites were prepared using a Haake, co-rotating, intermeshing twin screw extruder (diameter = 30 mm, $L/D = 10$) using a barrel temperature of 200 °C, a screw speed of 280 rpm, and a feed rate of 1200 g/h. Surlyn® materials were dried in a vacuum oven at 65 °C for a minimum of 48 hours prior to compounding while the organoclays were used as received. In prior studies from this laboratory [25,26], the amount of montmorillonite in the nanocomposite was determined by placing pre-dried nanocomposite pellets in a furnace at 900 °C for 45 min and weighing the remaining MMT ash. It was not possible to employ this technique with these ionomers since the polymer itself resulted in a hard, yellowish green coating on the inside of the crucible reflecting some complex residue of the inorganic component. The amount of the residue varied from batch to batch rendering this method useless for quantitative analysis. Hence, in order to ensure that a predetermined polymer/MMT ratio was maintained in all cases, the desired amounts of clay and polymer were premixed before feeding to the extruder and precautions were taken to minimize any losses during the extrusion process.

Tensile specimens (ASTM D638) and Izod specimens (ASTM D256) were prepared by injection molding using an Arburg Allrounder 305-210-700 injection molding machine using a barrel temperature of 220 °C, mold temperature of 45 °C, injection pressure of 70 bar and a holding pressure of 40 bar. After molding, the samples were immediately sealed in a polyethylene bag and placed in a vacuum desiccator for a minimum of 24 h prior to testing.

2.3. Testing and characterization

Tensile tests were conducted at room temperature according to ASTM D696 using an Instron model 1137 machine equipped with digital data acquisition capabilities. Modulus was measured using an extensiometer at a crosshead speed of 0.51 cm/min. Elongation at break, yield strength and tensile strength at break were measured at a crosshead speed of 5.1 cm/min. Typically, data from six specimens were averaged to determine the tensile properties with standard deviations of the order of 1–6% for modulus, 2% for yield strength and, 2–22% for elongation at break. Notched Izod impact tests were performed at room temperature using a TMI Izod tester (6.8 J hammer and 3.5 m/s impact velocity) according to ASTM D256. It is a common practice to cut the Izod bars into half (to generate more samples) and average the impact strength data from the 'gate end' (the end from which molten polymer enters the mold during injection molding) and the 'far end'. However, in multi-component systems, morphological differences can lead to significant differences between the impact strength measured at the gate end and the far end of a sample. Hence, in this study, the impact strength data from four samples each from the gate end and the far end of the bar were averaged separately; the standard deviation of these values was in the range of 2–18%.

WAXD was conducted using a Sintag XDS 2000 diffractometer in the reflection mode with an incident X-ray wavelength of 1.542 Å at a scan rate of 1.0 °/min. X-ray analysis was performed at room temperature on injection molded Izod bars. In order to see if there were any differences between the morphologies of the skin (surface) and the core, two sets of samples were prepared. The first set of samples used for studying the morphology of the skin, comprised of unmodified Izod bars of nanocomposites (thickness = 0.125 inches). The second set of samples used for studying the morphology of the core comprised of Izod bars that were milled down to a thickness of 0.065 inches using a Bridgeport® vertical mill. The specimens were oriented such that the incident beam reflected off the major face.

Samples for TEM analysis were taken from the core portion of an Izod bar parallel to the flow direction but perpendicular to the major face. Ultra-thin sections approximately 50 nm in thickness were cut with a diamond knife at a temperature of −40 °C using a Reichert-Jung Ultracut E microtome. Sections were collected on 300 mesh grids and subsequently dried with filter paper. These were then examined using a JEOL 2010F TEM equipped with a Field Emission Gun at an accelerating voltage of 120 kV.

Table 3
Tensile modulus of nanocomposites of selected grades of Surlyn® ionomers

Ionomer grade	Clay content	Tensile modulus (GPa)	
		$M_3(C_{18})_1$ organoclay	$M_2(HT)_2$-95 organoclay
Surlyn® 8920	0.0	0.252	0.252
	2.5	0.326	0.352
	5.0	0.371	0.473
	10.0	0.506	0.744
Surlyn® 8940	0.0	0.370	0.370
	2.0	0.425	0.433
	6.0	0.503	0.581
	12.0	0.669	0.940
Surlyn® 8945	0.0	0.262	0.262
	2.5	0.358	0.403
	5.0	0.423	0.560
	10.0	0.573	0.919

3. Selection of matrix polymer

The three grades of ionomers were melt mixed with $M_3(C_{18})_1$ and $M_2(HT)_2$ organoclays to form nanocomposites. The modulus data for these composites are listed in Table 3. The relative improvements in stiffness achieved, a measure of organoclay exfoliation, is plotted as a function of the clay content in Fig. 1. As is clearly evident, Surlyn® 8945 does a much better job of exfoliating the two-tailed organoclay than the other two polymers. Similar trends were seen with the one tailed organoclay, $M_3(C_{18})_1$, as shown in Table 3. Based on these analyses, Surlyn® 8945 was chosen as a matrix polymer for evaluating the effect of the structure of the surfactant on organoclay exfoliation.

We realize that any of the structural aspects of an ionomer matrix, viz., melt index, acid content, type of acid, degree of neutralization, and type of neutralizing ion (Na^+, Zn^{++}, Mg^{++}) could have a marked impact on its ability to exfoliate the organoclays. However, the objective of this study is not to design the best ionomeric polymer for preparing nanocomposites but to determine the best organoclay for use with a given ionomeric matrix.

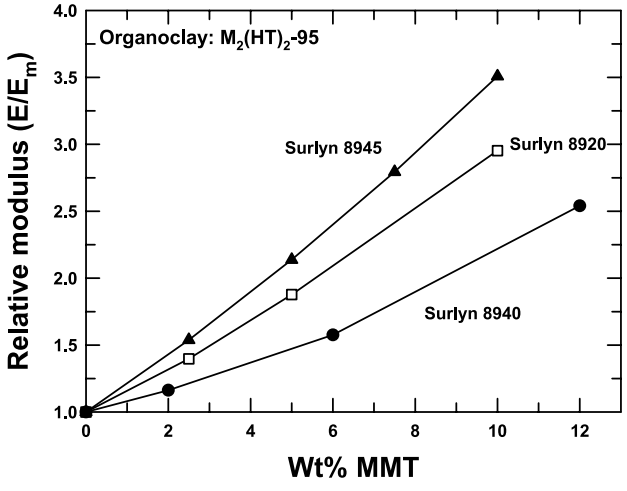

Fig. 1. Relative modulus as a function of montmorillonite content for nanocomposites prepared from three different grades of Surlyn® ionomer and $M_2(HT)_2-95$ organoclay.

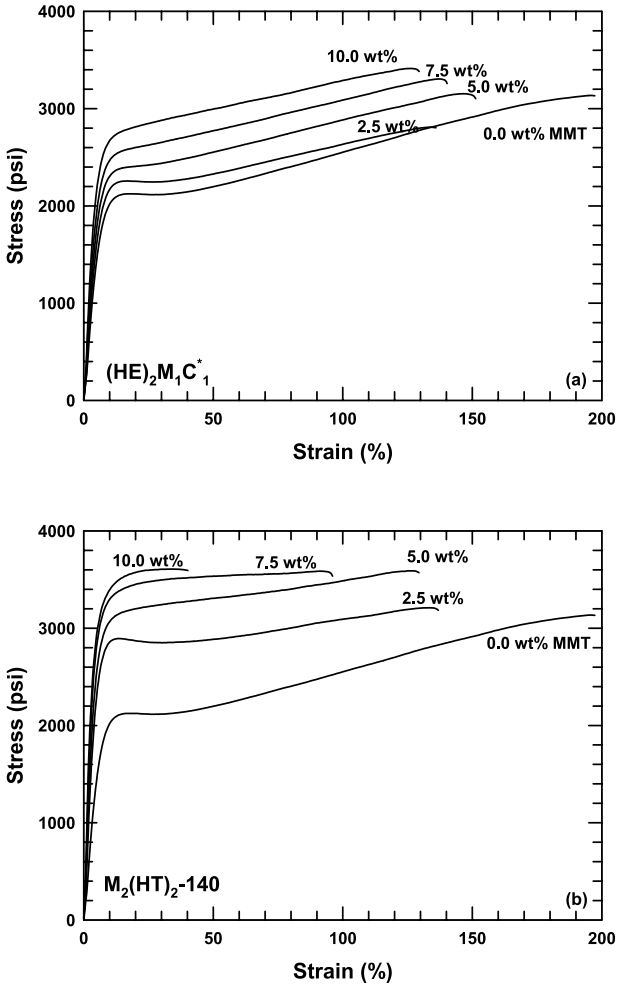

Fig. 2. Stress–strain diagrams of nanocomposites prepared from poly (ethylene-*co*-methacrylic acid) ionomer and (a) $(HE)_2M_1C_1^*$ and (b) $M_2(HT)_2$-140 organoclays measured at a crosshead speed of 5.1 cm/min.

4. Effect of organoclay structure on nanocomposite morphology and mechanical properties

4.1. Stress–strain analysis

Selected mechanical properties of Surlyn® 8945 based nanocomposites prepared with various organoclays are listed in Table 4. Differences in the enhancement of mechanical properties achieved with the addition of various organoclays reflect the variation in the extent of exfoliation attained in each of them. However, before we discuss these issues in detail, it is important to highlight the similarities and subtle differences in the stress–strain behavior of composites prepared from these organoclays. As an example, Fig. 2 displays the stress–strain diagrams for nanocomposites based on $(HE)_2M_1C_1^*$ and $M_2(HT)_2$-140,

Table 4
Select mechanical properties of nanocomposites formed from Surlyn® 8945 and various organoclays

Clay	Loading (% MMT)	Modulus (GPa)	Yield strength (5.1 cm/min) (MPa)	Tensile strength at break (5.1 cm/min) (MPa)	Elong. at break (5.1 cm/min) (%)	α[a]	Izod impact[b]	
							(Far end) (J/m)	(Gate end) (J/m)
None	0.0	0.262	14.5	21.3	194	7.31	442	428
$M_3(HT)_1$	2.5	0.349	17.9	21.2	117	6.22	573	601
	5.0	0.410	18.7	21.0	111	4.96	415	572
	7.5	0.465	19.6	22.1	119	3.96	294	491
	10.0	0.563	21.6	23.2	116	3.45	160	394
$M_3(C_{16})_1$	2.5	0.384	18.2	20.7	159	5.85	437	475
	5.0	0.452	18.4	22.3	155	5.37	328	478
	7.5	0.502	18.6	23.2	158	5.29	183	411
	10.0	0.544	19.9	23.6	140	5.26	119	319
$M_2(HT)_2$-95	2.5	0.403	18.9	22.3	127	6.21	572	675
	5.0	0.560	21.0	23.8	111	5.40	419	607
	7.5	0.732	23.8	26.6	72	4.68	109	249
	10.0	0.919	27.6	29.4	65	0.00	22*	43*
$M_2(HT)_2$-140	2.5	0.554	20.0	22.1	132	5.15	547	576
	5.0	0.628	21.7	25.5	131	4.04	162	422
	7.5	0.825	23.8	24.5	93	1.20	43	92
	10.0	1.008	24.1	24.9	42	0.00	17*	25*
$M_1(C_{16})_3$	2.5	0.498	20.4	25.2	148	6.53	641	685
	5.0	0.708	23.6	26.2	116	4.55	296	652
	7.5	0.857	26.7	27.2	63	0.00	95	237
	10.0	1.126	29.4	29.0	48	0.00	24*	98*
$(HE)_2M_1C_1^*$	2.5	0.328	15.9	19.6	145	6.60	483	422
	5.0	0.364	16.5	21.6	150	6.44	479	449
	7.5	0.419	17.9	23.4	148	6.46	359	462
	10.0	0.504	19.0	24.1	146	6.09	283	458
$(HE)_2M_1T_1$	2.5	0.396	18.5	22.5	145	6.15	490	587
	5.0	0.559	21.0	23.0	105	4.69	461	530
	7.5	0.708	23.5	25.3	106	4.29	323	439
	10.0	0.853	25.4	26.3	92	2.57	105	241
M_3T_1	2.5	0.385	18.2	22.3	164	6.01	397	408
	5.0	0.444	18.7	23.3	162	5.96	318	479
	7.5	0.489	19.3	22.7	150	5.26	209	460
	10.0	0.533	20.3	22.4	133	4.41	121	401
$M_1H_1(HT)_2$	2.5	0.413	19.0	24.2	180	6.20	536	535
	5.0	0.529	20.1	25.7	197	5.66	429	528
	7.5	0.695	22.0	25.0	174	4.99	304	468
	10.0	0.830	23.3	23.3	105	0.00	50	250

[a] α = Slope of the plastic region of the experimental stress–strain curve.
[b] An asterisk (*) denotes brittle failure.

two clays which cause significantly different degrees of matrix reinforcement. In both cases, at low clay concentrations, there is a distinct drop in the tensile stress after the yield point, corresponding to the onset of necking. This stress drop gradually diminishes as the clay content increases. Noticeably, the slope of the plastic region of the curves, indicative of strain hardening is different in both cases. Metallurgists typically quantify strain hardening by a 'strain hardening coefficient' n, defined as the slope of the plastic portion of the true stress–strain curve. However, because of the neck formation in test samples when subjected to uniaxial tension, it is difficult to determine the true stress–strain behavior for most polymer samples. A number of investigators have used non-contacting, imaging methods [27–30] to calculate the dynamic changes in the dimensions of samples during tensile testing and have, thus, determined their true stress–strain behavior. Since our labs are not equipped to perform such analyses, we define here an 'experimental strain hardening coefficient', α, as the slope of the plastic region of the experimental stress–strain curve. We realize that the absolute value of α may differ from that of n; however, α should provide a relative tool for comparing strain hardening in different nanocomposites. Fig. 3 shows the variation in strain hardening along with the clay concentration for $(HE)_2M_1C_1^*$ and $M_2(HT)_2$-140 based nanocomposites. The value of α drops precipitously at higher MMT concentrations for $M_2(HT)_2$-140 based nanocomposites compared to $(HE)_2M_1C_1^*$ based composites. The α values of all nanocomposites made are listed in Table 4. It appears that composites made from organoclays

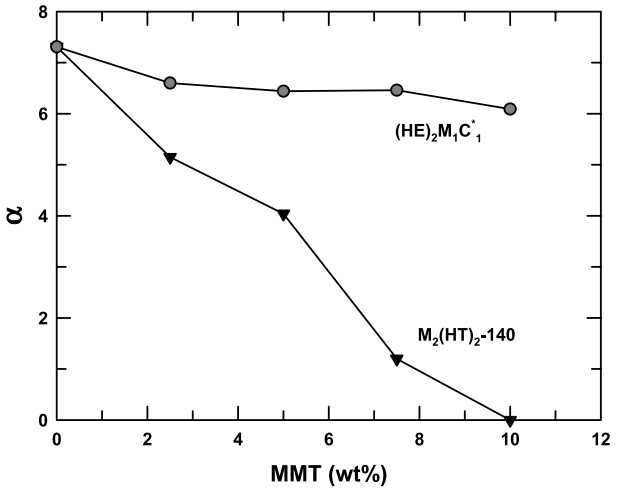

Fig. 3. Variation in the 'experimental strain hardening coefficient' α with clay concentration for nanocomposites prepared from $(HE)_2M_1C_1^*$ and $M_2(HT)_2$-140 organoclays.

that lead to high levels of reinforcement exhibit low degrees of strain hardening and vice versa.

4.2. Effect of the number of long alkyl groups on organoclay exfoliation

Fig. 4 shows TEM micrographs comparing the morphology of nanocomposites formed from Surlyn® 8945 and organoclays with one alkyl tail ($M_3(HT)_1$, $M_3(C_{16})_1$), two alkyl tails ($M_2(HT)_2$-95), and three alkyl tails ($M_1(C_{16})_3$). Nanocomposites from $M_2(HT)_2$-95 (Fig. 4(b)) exhibit a much better degree of clay exfoliation and distribution compared to those made from $M_3(HT)_1$ (Fig. 4(a)), which display a large number of unexfoliated clay tactoids. Similarly, the TEM micrograph of a composite made from $M_1(C_{16})_3$ shown in Fig. 4(d) reveals a higher level of exfoliation than that obtained for a nanocomposite made from a corresponding one-tailed organoclay $M_3(C_{16})_1$ (Fig. 4(c)).

The TEM analyses clearly corroborate the mechanical

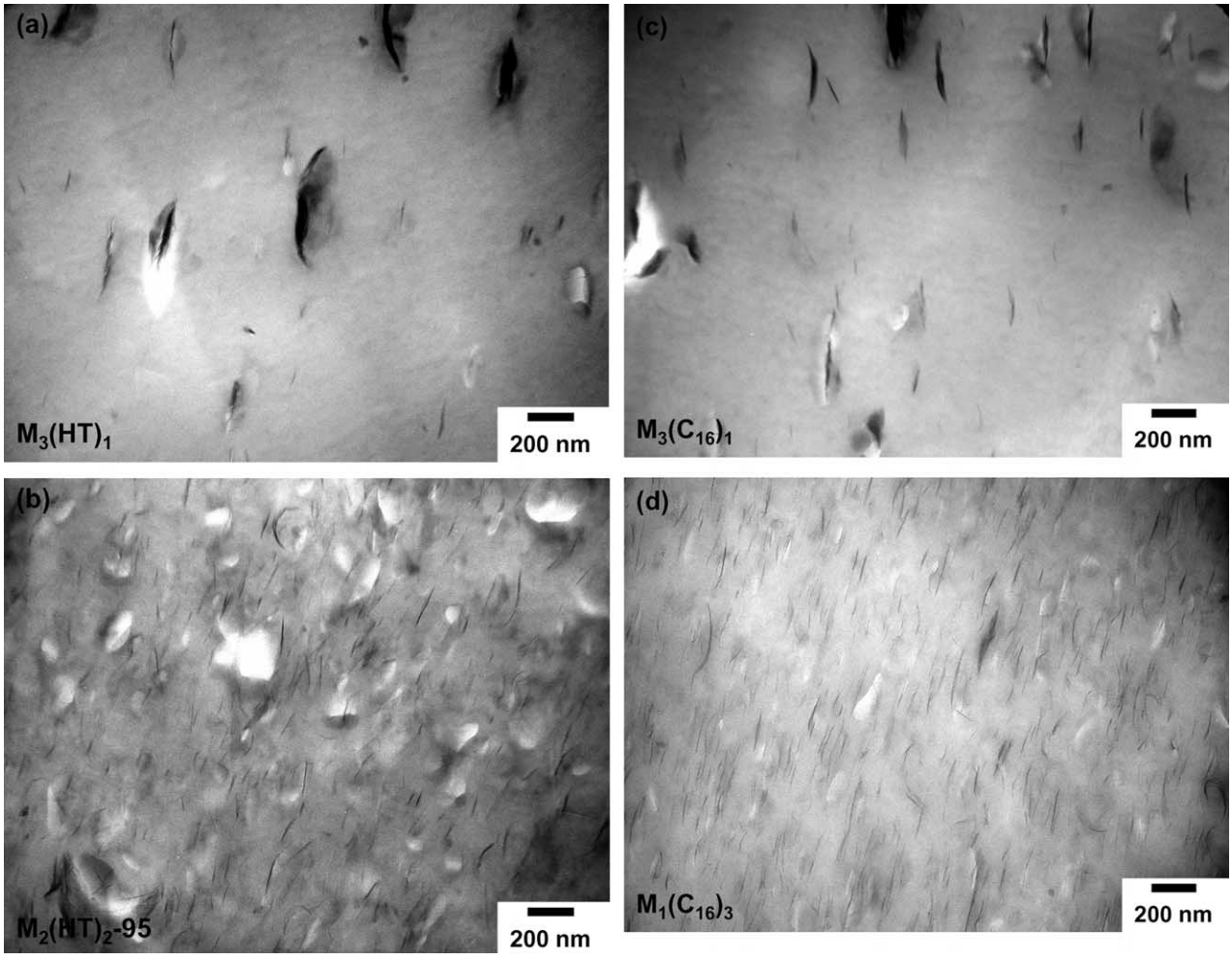

Fig. 4. TEM micrographs comparing the morphology of nanocomposites prepared from (a) a one-tailed organoclay, $M_3(HT)_1$, (b) two- tailed organoclay, $M_2(HT)_2$-95, (c) one-tailed organoclay, $M_3(C_{16})_1$, and (d) three tailed organoclay, $M_1(C_{16})_3$. The concentration of MMT in all cases is 2.5 wt%.

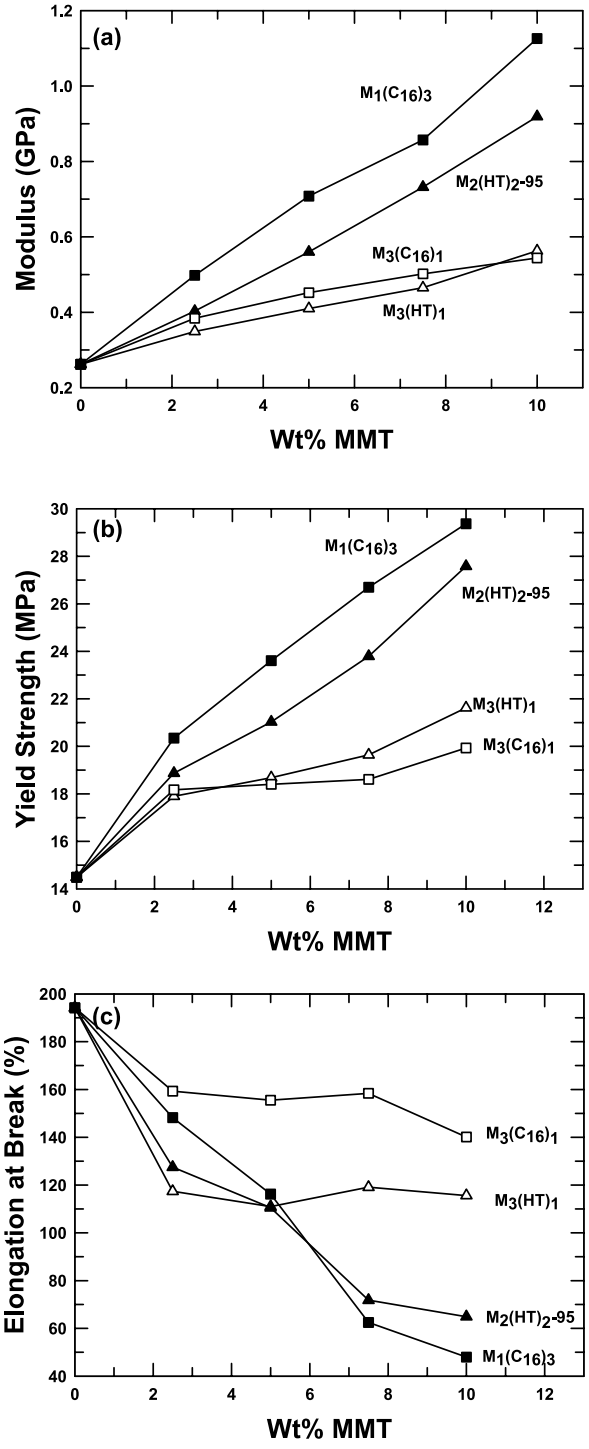

Fig. 5. (a) Tensile modulus, (b) yield strength, and (c) elongation at break of nanocomposites of poly(ethylene-*co*-methacrylic acid) ionomer showing the effect of the number of organoclay alkyl tails on nanocomposite mechanical properties.

property trends of these nanocomposites. Fig. 5(a) shows that the larger the number of alkyl tails, the higher the level of reinforcement. The increase in modulus on addition of MMT is much stronger for the organoclay with three alkyl tails $M_1(C_{16})_3$, than for one with two alkyl tails, $M_2(HT)_2$-95, which in turn is better than for those with one alkyl tail. There is not much difference between the moduli of the nanocomposites formed from the two one-tailed organoclays, $M_3(HT)_1$ and $M_3(C_{16})_1$. Yield strength data showed similar trends (Fig. 5(b)). Elongation at break data, presented in Fig. 5(c), show that the more exfoliated systems ($M_1(C_{16})_3$, $M_2(HT)_2$-95) are less ductile than the one-tailed systems; generally, ductility decreases when stiffness is increased by reinforcement.

Based on the above results, it is concluded that organoclays with multiple long alkyl groups lead to better exfoliation of montmorillonite platelets in these ionomers than organoclays with one long alkyl group when all other aspects of the structure are the same. This conclusion is similar to that made for LLDPE nanocomposites [7] but is opposite of that made for nylon 6 nanocomposites; where one alkyl tail leads to much better dispersion of clay than does two tails [23]. It is believed that nylon 6 has a higher affinity for the pristine surface of the organoclay than for the largely aliphatic organic modifier. The one-tailed surfactant leaves a large silicate surface area exposed for interaction with the polyamide and requires the polyamide to mix with fewer alkyl tails; whereas, the two tailed modifier shields more silicate surface and, thus, precludes desirable interactions between the polyamide and the clay surface, which ultimately limits the degree of organoclay exfoliation. In the case of poly(ethylene-*co*-methacrylic acid) ionomers, it could be argued that the polymer has a higher affinity for the alkyl tails than the silicate surface. As a result, the larger the number of alkyl tails, the larger is the number of relatively more favorable alkyl–polymer interactions and the more the silicate surface is shielded from the matrix, both of which leads to better exfoliation. Also, an increase in the number of alkyl tails increases the interplatelet distances within the clay tactoids and, thus, facilitates easier intercalation of the polymer within the clay galleries.

4.3. Effect of hydroxy-ethyl versus methyl groups on organoclay exfoliation

Fig. 6 shows TEM micrographs for nanocomposites based on organoclays with and without 2-hydroxy-ethyl substituents, i.e., $(HE)_2M_1T_1$ and M_3T_1. The micrographs expressly reveal a partially exfoliated morphology for the $(HE)_2M_1T_1$ based nanocomposites and an unexfoliated structure for the M_3T_1 based composites. The mechanical properties of the two types of nanocomposites parallel the TEM results. Fig. 7(a) shows that the organoclay from $(HE)_2M_1T_1$ surfactant leads to much higher levels of reinforcement than that from the M_3T_1 surfactant. The yield strength data, Fig. 7(b) and the elongation at break data, Fig. 7(c), agree well with the modulus data and electron micrographs.

The above analysis allows us to conclude that hydroxy-ethyl groups leads to better exfoliation of the clays in this matrix, which again is the opposite of what is seen in nylon

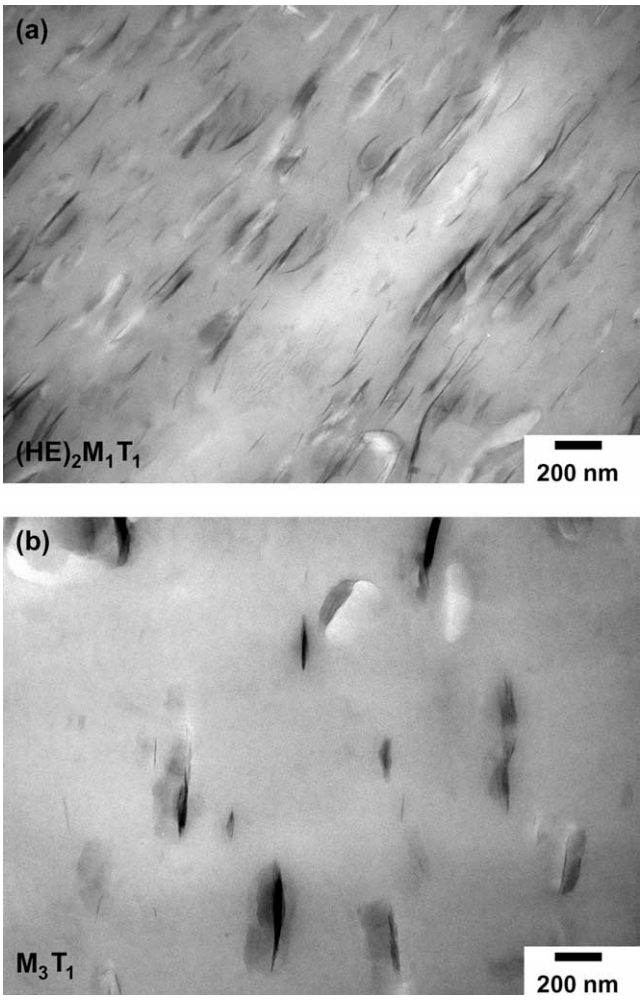

Fig. 6. TEM micrographs showing the morphology of nanocomposites formed from poly(ethylene-*co*-methacrylic acid) ionomer and the organoclays $(HE)_2M_1T_1$ and M_3T_1. The concentration of MMT in both cases is 5.0 wt%.

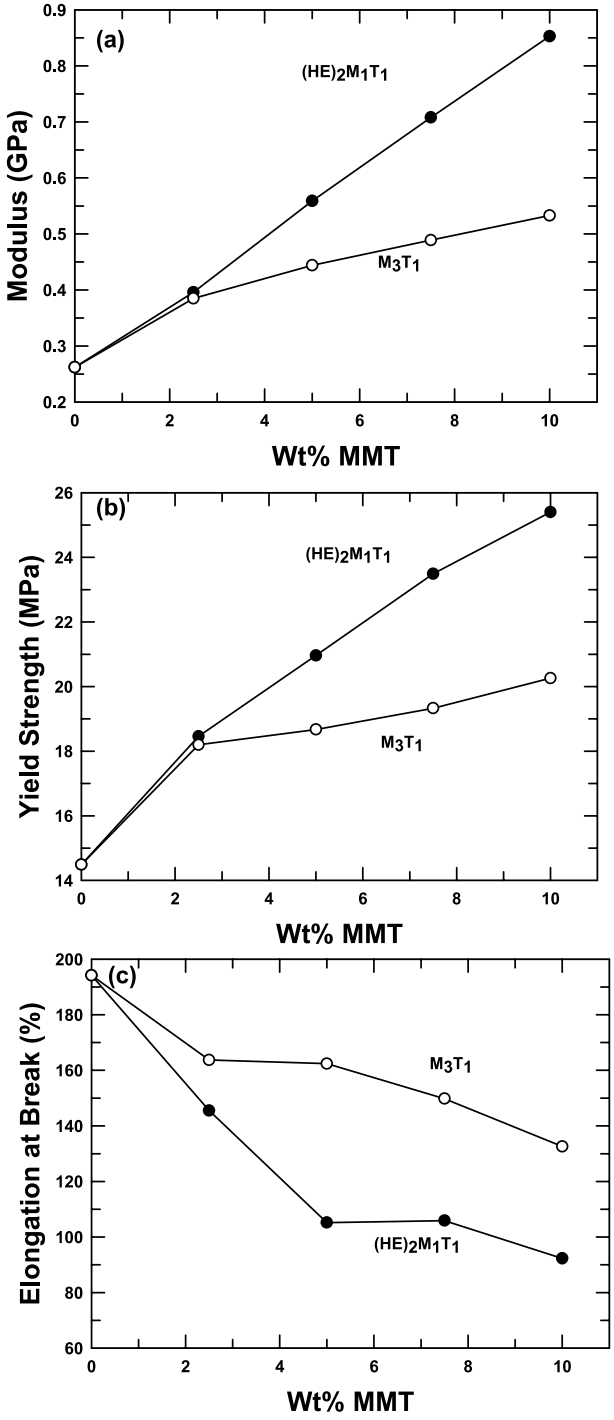

Fig. 7. (a) Tensile modulus, (b) yield strength, and (c) elongation at break of nanocomposites of poly(ethylene-*co*-methacrylic acid) ionomer showing the effect of 2-hydroxy-ethyl versus methyl groups on nanocomposite mechanical properties.

6 based nanocomposites. The differences in morphology and mechanical properties between the composites of the two organoclays are surprisingly large and unprecedented. The improved exfoliation in the case of the $(HE)_2M_1T_1$ organoclay in this matrix could be the combined effect of (i) the favorable chemical interactions between the hydroxyl groups of the surfactant and the ionic or acid groups of the polymer and (ii) reduction of the unfavorable polymer-silicate interactions. The larger hydroxy-ethyl groups occupy more space than the methyl substituents. In addition, the –OH moiety may prefer to reside flat on the surface due to attraction to oxygen atoms on the clay. Larger shielding of the clay surface by $(HE)_2M_1T_1$ surfactant, reduces the polymer–clay contact area and, thus, leads to improved exfoliation.

4.4. Effect of the length of the surfactant alkyl tail on organoclay exfoliation

The TEM micrographs in Fig. 8 provide comparison between the morphology of nanocomposites prepared from organoclays with two different tail lengths. Although, both $(HE)_2M_1T_1$ and $(HE)_2M_1C_1^*$ clays contain the favorable hydroxy-ethyl substituent, the $(HE)_2M_1T_1$ clay, which is predominantly comprised of C_{18} chains, leads to much

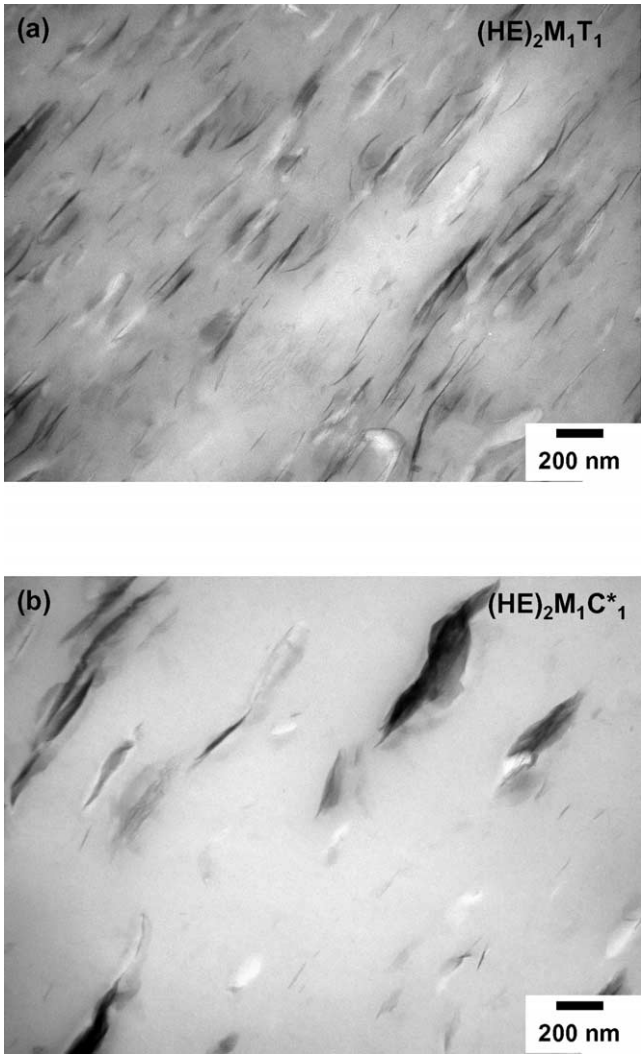

Fig. 8. TEM micrographs showing the morphology of nanocomposites formed from poly(ethylene-*co*-methacrylic acid) ionomer and the organoclays $(HE)_2M_1T_1$ and $(HE)_2M_1C^*_1$. The concentration of MMT in both cases is 5.0 wt%.

higher levels of platelet exfoliation than $(HE)_2M_1C^*_1$, which is comprised mainly of C_{12} chains. The mechanical property data are in congruence with the TEM analysis. The tensile moduli of the $(HE)_2M_1T_1$ based composites are about 20–70% higher than that of $(HE)_2M_1C^*_1$ based composites, with the differences being more pronounced at higher MMT concentrations as seen in Fig. 9(a). The yield strength (Fig. 9(b)), and the ductility data (Fig. 9(c)) agree well with the modulus trends.

These observations lead to the conclusion that surfactants with longer alkyl tails are better at exfoliating montmorillonite clays than those with a shorter alkyl tails. The shorter C_{12} tails of $(HE)_2M_1C^*_1$ organoclay result in a lower shielding efficiency and smaller inter-platelet distances as compared to $(HE)_2M_1T_1$ which evidently leads to lower levels of exfoliation.

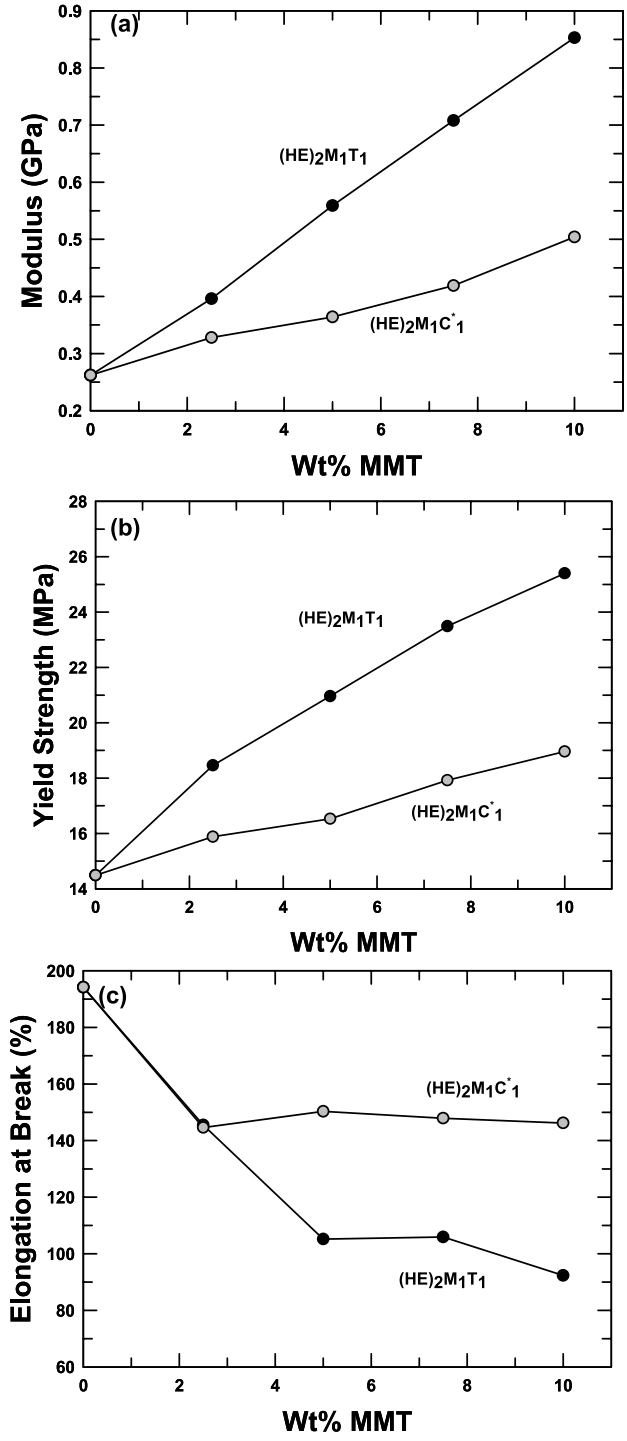

Fig. 9. (a) Tensile modulus, (b) yield strength, and (c) elongation at break of nanocomposites of poly(ethylene-*co*-methacrylic acid) ionomer showing the effect of the length of the alkyl tail on nanocomposite mechanical properties.

4.5. Effect of the level of organic loading on clay exfoliation (MER comparison)

TEM micrographs of the nanocomposites formed from $M_2(HT)_2$-95 and $M_2(HT)_2$-140, respectively, are shown in

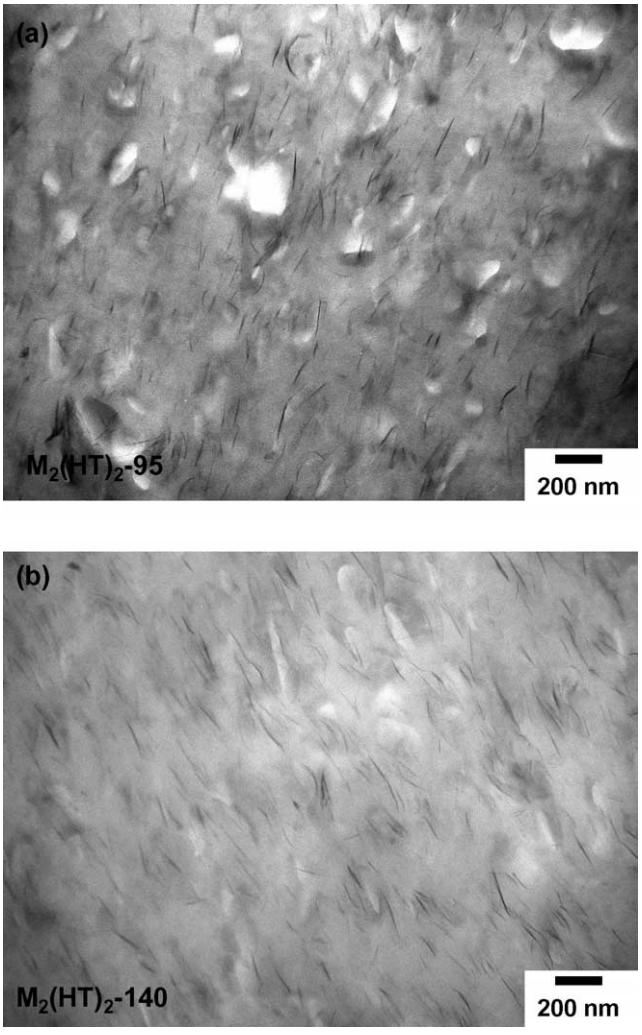

Fig. 10. TEM micrographs showing the morphology of nanocomposites formed from poly(ethylene-*co*-methacrylic acid) ionomer and the organoclays $M_2(HT)_2$-95 and $M_2(HT)_2$-140. The concentration of MMT in both cases is 2.5 wt%.

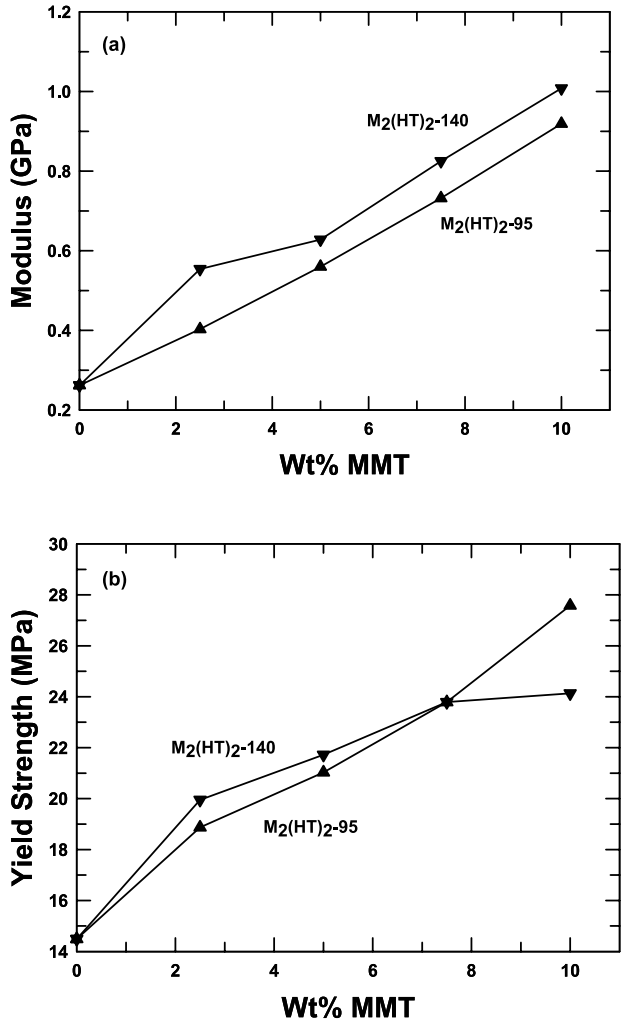

Fig. 11. (a) Tensile modulus and (b) yield strength of poly(ethylene-*co*-methacrylic acid) ionomer showing the effect of MER loading on nanocomposite mechanical properties.

Fig. 10. In both cases a partially exfoliated morphology consisting of individual silicate platelets along with stacks containing two to five platelets is seen. The mechanical properties, however, do provide a clearer and more meaningful distinction between the two organoclays. As seen in Fig. 11(a), the improvement in modulus values achieved with the over-exchanged clay, $M_2(HT)_2$-140, is roughly 10–15% more than that achieved with $M_2(HT)_2$-95. This trend is the opposite of what is seen in nylon 6 composites. It appears that the increased alkyl–ionomer interactions and higher inter-platelet distances resulting from the over-exchange of the surfactant helps in improving exfoliation in this matrix. Chemical interchanges between the Na^+ cation of the ionomer and the amine cation of the freely available surfactant could also be contributing to this effect. The improvement in yield strength also follows a similar trend except at high organoclay concentrations, where the yield strength for $M_2(HT)_2$-140 based composites is lower than that of $M_2(HT)_2$-95 based composites (Fig. 11(b)). We believe this to be a result of a weaker clay–polymer interface caused by the excessive surfactant available at higher organoclay concentrations. Further elaboration on clay–matrix adhesion are made in Discussion.

4.6. Saturated tallow effects

The long alkyl tails on the surfactants are made from natural oils that contain a certain level of unsaturation. This unsaturation may lead to undesired chemical reactions like matrix degradation [24] at the high temperatures used in melt processing. To examine these effects, nanocomposites based on the saturated and unsaturated form of tallow, $M_3(HT)_1$ and M_3T_1, respectively, were compared against each other. As shown in Fig. 12, the TEM micrographs show no significant differences in the morphology of the two composites. In both cases, the micrographs reveal similar unaltered clay stacks. The mechanical property values of the

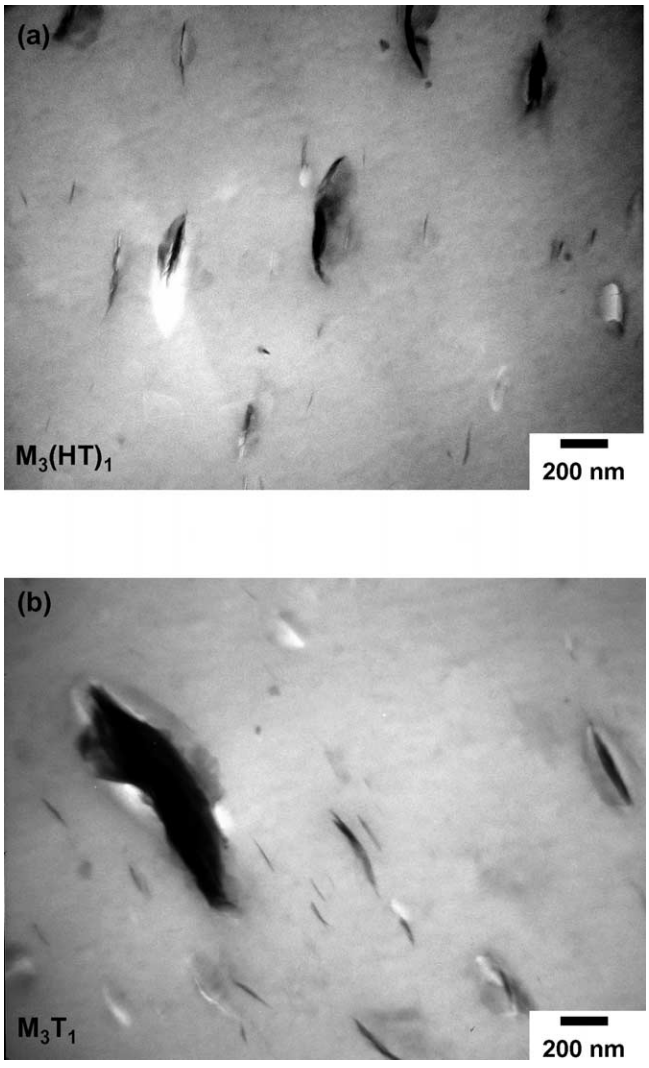

Fig. 12. TEM micrographs showing the morphology of nanocomposites formed from poly(ethylene-*co*-methacrylic acid) ionomer and the organoclays $(HE)_2M_1T_1$ and M_3T_1. The concentration of MMT in both cases is 2.5 wt%.

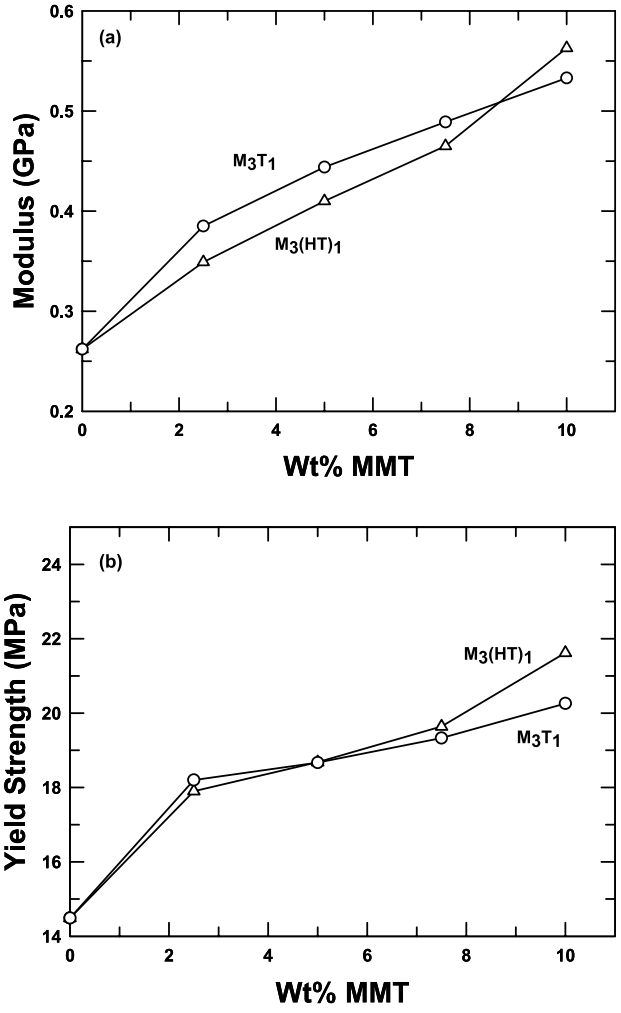

Fig. 13. (a) Tensile modulus and (b) yield strength of nanocomposites of poly(ethylene-*co*-methacrylic acid) ionomer showing the effect of alkyl saturation on nanocomposite mechanical properties.

two nanocomposites are also similar. Modulus results shown in Fig. 13(a) reveal a slight advantage for the unsaturated clay at low MMT levels. The yield strength results, seen in Fig. 13(b), are nearly the same for the two composites. Based on these results, it appears that neither the nanocomposite structure nor its mechanical properties are much affected by the hydrogenation of the tallow double bonds for this system.

4.7. Effect of quaternary versus tertiary ammonium treatments

Fig. 14 compares the mechanical properties of nanocomposites made from an organoclay with a quaternary amine, $M_2(HT)_2$-95 to that with a tertiary amine, $M_1H_1(HT)_2$. Modulus results for the two composites, (Fig. 14(a)) are similar, although, ($M_2(HT)_2$-95) based composites seem to show slightly higher levels of reinforcement. The yield strength data follow a similar trend, Fig. 14(b). The use of a quaternary amine over a tertiary amine seems to have no sizable effect on the nanocomposite mechanical properties. The small advantage displayed by $M_2(HT)_2$-95 based composites may be the result of the slightly better shielding ability of the bulkier methyl group as compared to the hydrogen group present in the tertiary amine.

4.8. WAXS analysis

As mentioned in Testing and characterization section, two sets of samples were prepared to differentiate between the WAXD patterns and, thus, the morphologies of the skin (surface) and the core of the ionomer based nanocomposites. The WAXD patterns of the skin of selected nanocomposites prepared with different organoclays are presented in Fig. 15. All of these patterns show a distinct peak indicative of the presence of unexfoliated clay tactoids. However, the position of the peaks has shifted in different

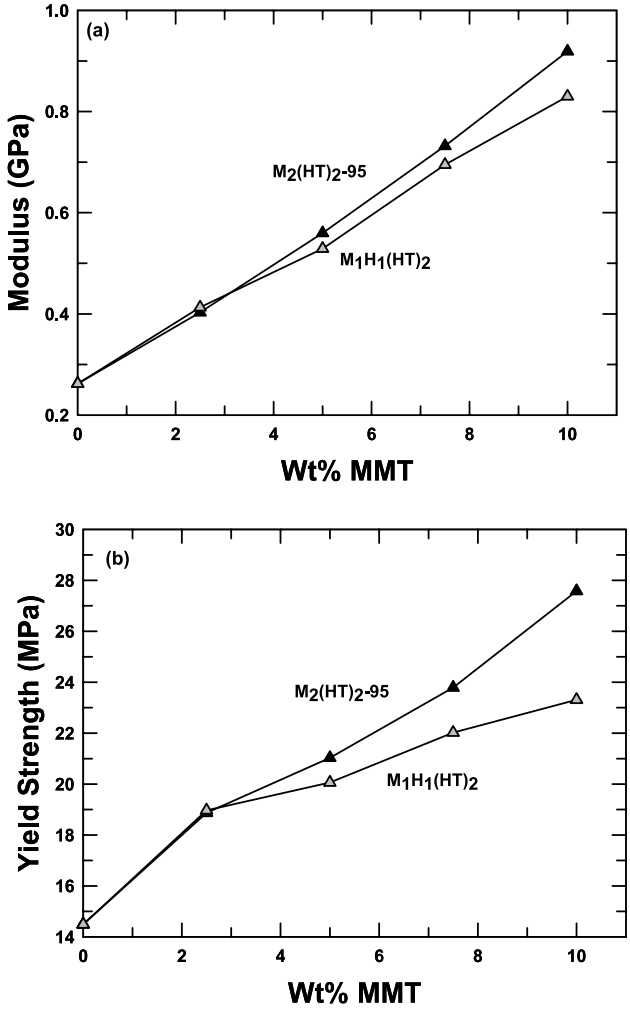

Fig. 14. (a) Tensile modulus and (b) yield strength of nanocomposites of poly(ethylene-*co*-methacrylic acid) ionomer showing the effect of quaternary versus tertiary amines on nanocomposite mechanical properties.

directions when compared to the WAXD patterns of the organoclays from which they were prepared (Fig. 16). The peaks of the composites formed from the two-tailed and three-tailed nanocomposites have shifted to higher *d*-spacings than the organoclays, which according to prevalent understanding suggests the intercalation of polymer within the clay galleries. On the other hand, XRD patterns of nanocomposites prepared from one tailed organoclays revealed a peak that had shifted to the right hand side (lower *d*-spacings) which could be a result of surfactant degradation. Similar peak shifts to lower *d*-spacings have been reported for LLDPE [7] and nylon 66 [31] based nanocomposites as well as for highly concentrated masterbatches of nylon 6 nanocomposites [25].

Fig. 17 compares WAXD scans from the core of Izod bars prepared from selected nanocomposites based on different organoclays. A comparison of Figs. 15 and 17 reveals a much lower X-ray scattering intensity from the core samples than from the skin samples; note the more expanded intensity scale in Fig. 17 than Fig. 15 and the resulting higher noise to signal ratio. We believe, the high level of platelet orientation in the skin, resulting from the shear stresses along the walls of the mold during injection molding, than in the core explains these differences. The scans from the core of nanocomposites prepared from $M_2(HT)_2$-95, $M_2(HT)_2$-140, $M_1(C_{16})_3$, $(HE)_2M_1T_1$ organoclays were devoid of any characteristic peaks which is often interpreted as a sign of complete exfoliation. However, we believe this lack of an X-ray peak is the result of a more random orientation of clay particles rather than indicating a more exfoliated morphology; TEM analyses support this hypothesis. X-ray scans of corresponding samples made from $(HE)_2M_1C_1^*$ and $M_3(C_{16})_1$ organoclays have a distinct peak suggesting that these systems have a relatively larger number of unexfoliated clay bundles. This agrees well with the mechanical property and TEM analyses. For a given organoclay, the position of the peak was the same in the skin and the core, however, the height of the peak increased with an increase in the clay concentration.

4.9. Izod Impact measurements

The effects of the clay type and content on room temperature Izod impact behavior of nanocomposites of poly(ethylene-*co*-methacrylic acid) ionomers are presented in Table 4. Although, there is not much difference between the Izod impact values of the gate and far end samples for the neat polymer, the gate end samples are tougher than the far end samples for most nanocomposites. This is the opposite of what has been reported for rubber toughened polyamide blends [32], where the far end samples were found to be tougher than the gate end samples due to differences in the blend morphology at the two ends; rubber particles at the far end were found to be spherical while those at the gate end were highly elongated. In our case, these differences could be a result of possible differences in platelet orientation between the far end and the gate end. To illustrate the current trends, Fig. 18 shows a plot of the Izod behavior of $(HE)_2M_1T_1$ based nanocomposites versus MMT content. In most cases, the differences between the gate and far end are more pronounced at higher clay concentrations.

For all nanocomposites, toughness as judged by Izod improves with clay addition for low concentrations, but it deteriorates gradually with further increase in clay concentration. The drop in the Izod impact values observed at high clay concentrations is more precipitous in composites that exhibit good clay exfoliation. Since the Izod test measures the energy absorbed during impact, i.e., the area under the resisting force versus displacement curve during the test, as measured using instrumental impact test devices, the values obtained reflect a net result of opposing effects brought by the increased stiffness and reduced ductility. At low clay concentrations, improvements in Izod may reflect the increased stiffness and yield strength of the material which offset the negative effects brought by the drop in its ductility, i.e. extent of plastic deformation. However, at high

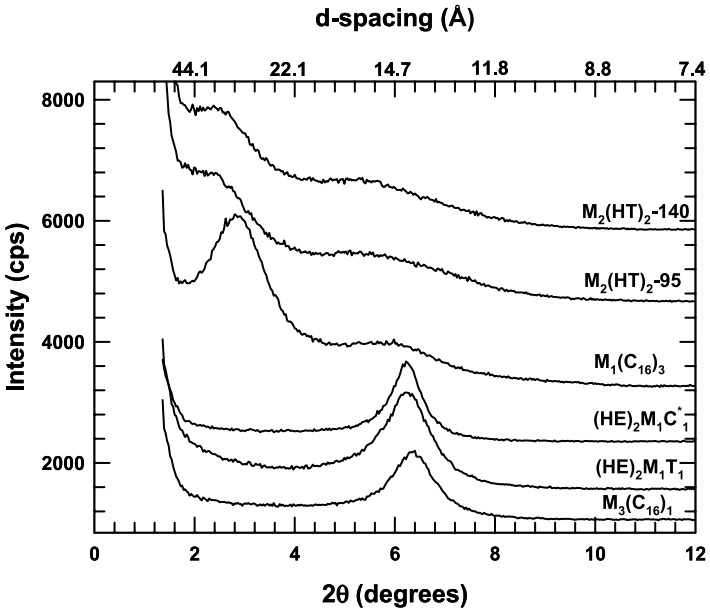

Fig. 15. WAXD patterns of the skin (surface) of injection molded nanocomposites formed from poly(ethylene-*co*-methacrylic acid) ionomer and various organoclays. The concentration of MMT in all cases is 5.0 wt%. The curves are shifted vertically for clarity.

clay concentrations, the decreased ductility seems to dominate and toughness decreases.

5. Discussion

As described above, a series of polymer–silicate nanocomposites were prepared by melt mixing poly(ethylene-*co*-methacrylic acid) ionomers with ten different organoclays. It should be noted that although some organoclays were exfoliated better than others, none of these nanocomposites exhibited exfoliation levels similar to those seen in nylon 6 nanocomposites. Fig. 19 shows the relative improvement in matrix stiffness achieved by melt mixing these organoclays with Surlyn® 8945 ionomer. It is clear that the addition of $M_1(C_{16})_3$ and $M_2(HT)_2$-140 result in the highest improvement in modulus, indicative of their higher levels of exfoliation as compared to the others. On the other hand, most one-tailed organoclays seem to form poorly exfoliated composites. The differences are more pronounced at higher organoclay concentrations, where large agglomerates of the order of a few microns were seen in nanocomposites made from one-tailed organoclays. The use of hydroxy-ethyl instead of methyl substituents clearly

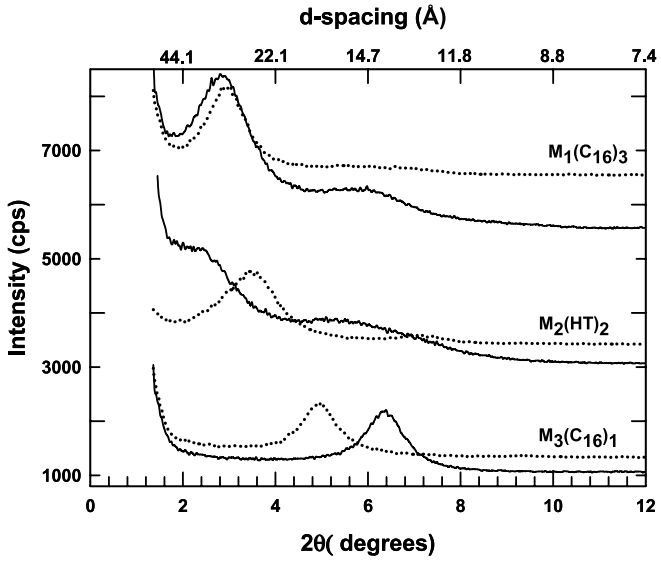

Fig. 16. WAXD patterns of the skin (surface) of nanocomposites formed from poly(ethylene-*co*-methacrylic acid) ionomer (full curves) and the corresponding organoclays used to prepare them (dotted curves). The concentration of MMT in all cases is 5.0 wt%. The curves are shifted vertically for clarity.

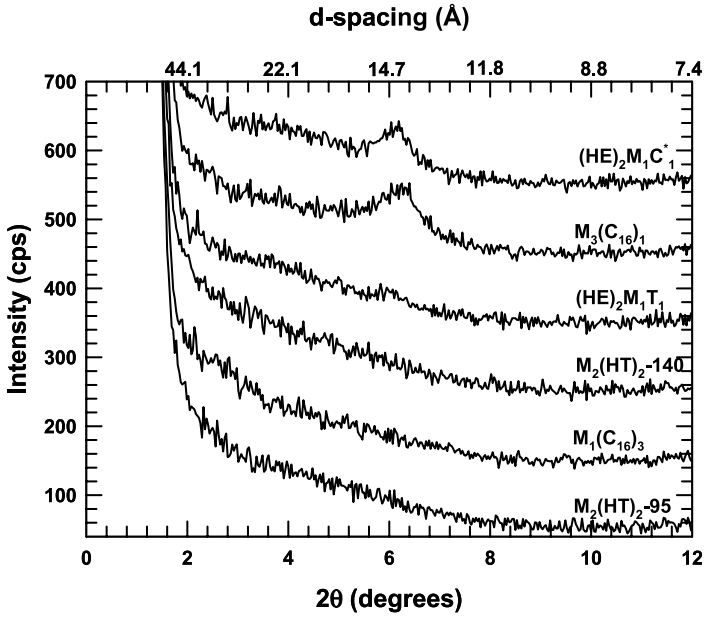

Fig. 17. WAXD patterns of the core of nanocomposites formed from poly(ethylene-*co*-methacrylic acid) ionomer and various organoclays. The concentration of MMT in all cases is 5.0 wt%. The curves are shifted vertically for clarity.

results in improved exfoliation. However, as seen in Fig. 19, the lower reinforcement levels observed in composites formed from $(HE)_2M_1C_1^*$ as compared to those from M_3T_1 indicates that the effect of the shorter alkyl tail length of $(HE)_2M_1C_1^*$ more than negates the favorable effects induced by the hydroxy-ethyl substituents. This suggests that in order to achieve better exfoliation, a longer alkyl tail is more critical than hydroxy-ethyl substitutions.

Fig. 20 shows a plot of the nanocomposite tensile modulus versus the organoclay *d*-spacing at 2.5 wt% MMT. Clearly, composites made from organoclays with larger *d*-spacings have higher moduli than composites formed from organoclays with smaller *d*-spacings. Similar trends were seen at higher clay concentrations. It could be argued that larger *d*-spacings facilitate easier intercalation of the ionomer within the clay galleries which may subsequently lead to better exfoliation of the clay and, thus, the higher modulus. However, instead of a direct cause and effect relationship, it is quite likely that both the higher stiffness and the larger *d*-spacings are a result of the higher alkyl content associated with multiple tails, long tails or excess surfactant.

The nanocomposite Izod impact values are plotted against the organoclay *d*-spacing in Fig. 21. At low clay concentrations, the Izod impact increases with increasing organoclay *d*-spacing as seen in Fig. 21(a). The higher increase in stiffness associated with the larger *d*-spacings (as shown in Fig. 20) results in higher energy absorption for

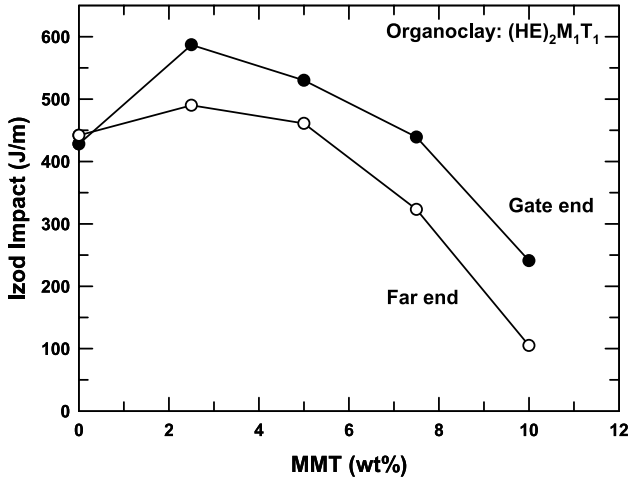

Fig. 18. Izod impact strength as a function of montmorillonite content for nanocomposites formed from poly(ethylene-*co*-methacrylic acid) ionomer and $(HE)_2M_1T_1$ organoclay.

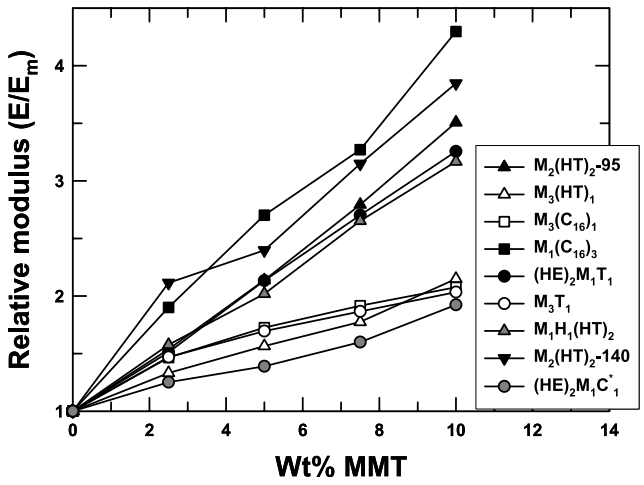

Fig. 19. Relative modulus (E/E_m) as a function of montmorillonite content for nanocomposites formed from poly(ethylene-*co*-methacrylic acid) ionomer and various organoclays.

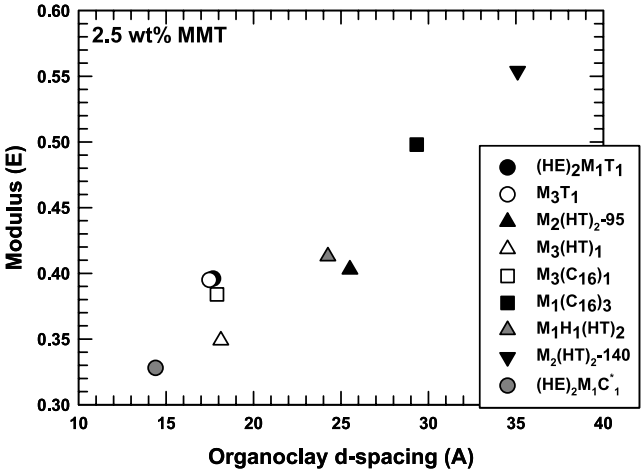

Fig. 20. Tensile modulus versus organoclay *d*-spacing for nanocomposites formed from poly(ethylene-*co*-methacrylic acid) ionomer and various organoclays.

these nanocomposites as compared to nanocomposites prepared from organoclays with smaller *d*-spacings. At high clay concentrations, the ductility of nanocomposites made from organoclays with large *d*-spacings, due to better exfoliation, drops dramatically and as a result the Izod impact trend reverses as shown in Fig. 21(b).

Adequate levels of filler-matrix adhesion are necessary for good performance of conventional composites based on glass or carbon fibers. Polymer-filler interfacial adhesion does not have a significant effect on the tensile modulus of composites, assuming fixed morphology; however, good adhesion is needed to build strength. To study these effects in ionomer–organoclay nanocomposites, we have plotted the yield strength against the modulus of these composites in Fig. 22. For most of the organoclays, the relationship between yield strength and modulus appears to be about the same which could imply that morphological rather than interfacial adhesion effects dominate in this series of systems. The only exception are nanocomposites formed

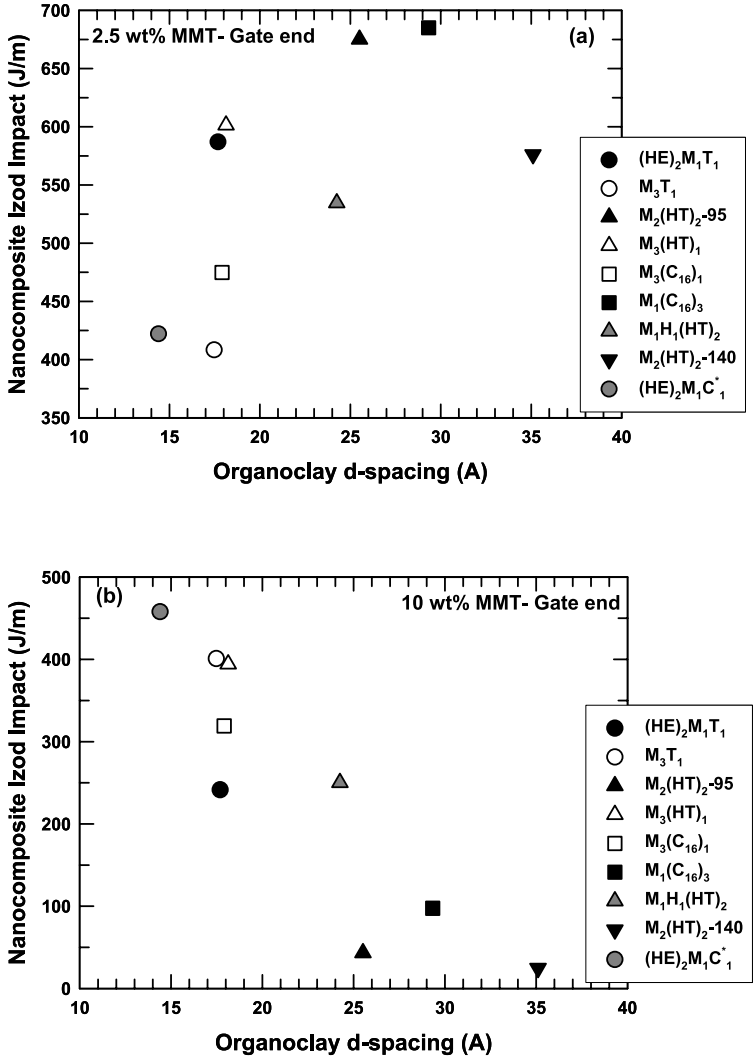

Fig. 21. Izod impact strength versus organoclay *d*-spacing for nanocomposites formed from poly(ethylene-*co*-methacrylic acid) ionomer and various organoclays at (a) 2.5 wt% MMT and (b) 10 wt% MMT.

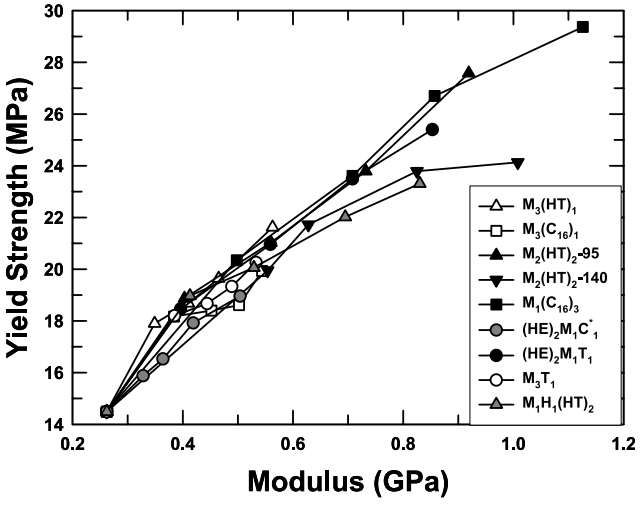

Fig. 22. Yield strength versus tensile modulus for nanocomposites formed from poly(ethylene-*co*-methacrylic acid) ionomer and various organoclays.

from $M_2(HT)_2$-140 clays, where at higher organoclay concentrations, the yield strength is lower than expected based on the value of modulus possibly indicating a weaker interface. We believe that the excess surfactant, which may interact well with the polymer but is not ionically bonded to the silica surface, might be a factor in this.

6. Conclusion

Structure–property relationships for nanocomposites formed by melt processing from a series of organoclays and poly(ethylene-*co*-methacrylic acid) ionomers are presented here. The chemical structure of the alkyl ammonium surfactants was systematically varied to determine how specific groups might affect the mechanical properties and morphology of these composites. Four distinct surfactant structural effects have been identified that lead to improved levels of exfoliation and higher stiffness for these nanocomposites: (1) higher number of alkyl tails on the amine rather than one, (2) longer alkyl tails instead of shorter ones, (3) 2-hydroxy-ethyl groups as opposed to methyl groups on the ammonium ion, and (4) excess amount of the amine surfactant on the clay instead of an equivalent amount. Most of these trends are opposite from what has been observed in nylon 6 based nanocomposites [20]. It seems nylon 6 has a higher affinity for the silicate surface than does the poly(ethylene-*co*-methacrylic acid) ionomer while the latter is less repelled by the alkyl tails than the polyamide. Hence, surfactant structural aspects that lead to more shielding of the silicate surface or increased alkyl material leads to improved exfoliation in the ionomer. These observations are similar to those seen with LDPE [10] and LLDPE [7] based nanocomposites. It should also be noted that, although some organoclays were exfoliated better than others, none of the ionomer-based nanocomposites exhibited exfoliation levels as great as those seen in nylon 6 nanocomposites. Thus, although addition of the acidic and ionic groups (present in ionomers) improves the matrix-polarity and, thus, organoclay exfoliation in polyethylene [10], this does not lead to as favorable polymer-organoclay interactions as observed for nylon 6 based nanocomposites. Nevertheless, nanocomposites prepared from such ionomers offer promising improvements in performance and may be particularly suitable for barrier applications.

It would be interesting to isolate the relative effects of the ionic and acid groups on exfoliation by comparing nanocomposites made from a series of materials with systematically varied structures. Such studies are currently in progress.

Acknowledgements

This work was funded by the Air Force Office of Scientific Research. The authors sincerely thank Southern Clay Products, Inc. for providing organoclay materials and WAXD analyses. We also acknowledge P. J. Yoon for numerous insightful discussions. We are thankful to Eddie Oliver and Jim Smitherman for their assistance in preparing samples for WAXD analyses and JiPing Zhou for his help on the TEM.

References

[1] Okada A, Fukushima Y, Kawasumi M, Inagaki S, Usuki A, Sugiyami S, Kurauchi T, Kamigaito O. United States Patent 4739007; 1988. [Assigned to Toyota Motor Co., Japan].
[2] Usuki A, Kojima Y, Kawasumi M, Okada A, Fukushima Y, Kurauchi T, Kamigaito O. J Mater Res 1993;8(5):1179–84.
[3] Christiani BR, Maxfield M. United States Patent 5747560; 1998. [Assigned to Allied Signal].
[4] Liu L, Qi Z, Zhu X. J Appl Polym Sci 1999;71(7):1133–8.
[5] Cho JW, Paul DR. Polymer 2001;42(3):1083–94.
[6] Hasegawa N, Kawasumi M, Kato M, Usuki A, Okada A. J Appl Polym Sci 1998;67(1):87–92.
[7] Hotta S, Paul DR. Polymer 2004;45(22):7639–54.
[8] Hasegawa N, Okamoto H, Kawasumi M, Kato M, Tsukigase A, Usuki A. Macromol Mater Eng 2000;280(281):76–9.
[9] Li X, Wang C-y, Fang L, Liu L-z. Harbin Ligong Daxue Xuebao 2003;8(2):90–3.
[10] Shah RK, Paul DR. In preparation.
[11] Kobayashi T, Takahashi T, Monma T, Kurosaka K, Arai T. WO Patent 9731973; 1997. [Assigned to (E. I. Du Pont de Nemours & Co., USA; Kunimine Industries Co., Ltd.)].
[12] Hasegawa N, Kawakado M, Usuki A, Okada A. JP Patent 97-152854; 1998. [Assigned to (Toyota Central Research and Development Laboratories, Inc., Japan).].
[13] Ding R-D, Newell C. U.S. Patent Application Publication US2003/0207984 A1;2003.
[14] Barber GD, Moore RB. Polym Mater Sci Eng 2000;82:241–2.
[15] Barber GD, Bellman SP, Moore RB. Annual Technical Conference—Society of Plastics Engineers 2003;61st(Vol. 2):1369–1373.
[16] Chisholm BJ, Moore RB, Barber G, Khouri F, Hempstead A, Larsen M, Olson E, Kelley J, Balch G, Caraher J. Macromolecules 2002;35(14):5508–16.

[17] Barber GD, Carter CM, Moore RB. Annual Technical Conference—Society of Plastics Engineers 2000;58th(Vol. 3):3763–3767.
[18] Start PR, Mauritz KA. J Polym Sci, Part B: Polym Phys 2003;41(13):1563–71.
[19] Kovarova L, Kalendova A, Malac J, Vaculik J, Malac Z, Simonik J. Annual Technical Conference—Society of Plastics Engineers 2002;60th(Vol. 2):2291–2295.
[20] Fornes TD, Yoon PJ, Hunter DL, Keskkula H, Paul DR. Polymer 2002;43(22):5915–33.
[21] Yoon PJ, Hunter DL, Paul DR. Polymer 2003;44(18):5323–39.
[22] Stretz HA, Paul DR. Polymer 2004; Submitted for publication.
[23] Fornes TD, Hunter DL, Paul DR. Macromolecules 2004;37(5):1793–8.
[24] Fornes TD, Yoon PJ, Paul DR. Polymer 2003;44(24):7545–56.
[25] Shah RK, Paul DR. Polymer 2004;45(9):2991–3000.
[26] Fornes TD, Yoon PJ, Keskkula H, Paul DR. Polymer 2001;42(25):9929–40.
[27] Nazarenko S, Bensason S, Hiltner A, Baer E. Polymer 1994;35(18):3883–92.
[28] Laraba-Abbes F, Ienny P, Piqules R. Kautschuk Gummi Kunststoffe 1999;52(3):209–14.
[29] Gloaguen JM, Lefebvre JM. Polymer 2001;42(13):5841–7.
[30] Haynes AR, Coates PD. J Mater Sci 1996;31(7):1843–55.
[31] Chavarria F, Paul DR. Polymer 2004; 45:8501–15.
[32] Huang JJ, Keskkula H, Paul DR. Polymer 2004;45(12):4203–15.